01 Sep 2016

# Numerical Modeling of Dust Dynamics around Small Asteroids

William Yu

Joseph J. Wang

Daoru Frank Han
*Missouri University of Science and Technology*, handao@mst.edu



## Recommended Citation

W. Yu et al., "Numerical Modeling of Dust Dynamics around Small Asteroids," *Proceedings of the AIAA Space and Astronautics Forum and Exposition, SPACE 2016 (2016, Long Beach, CA)*, American Institute of Aeronautics and Astronautics (AIAA), Sep 2016.
The definitive version is available at https://doi.org/10.2514/6.2016-5447

# Numerical Modeling of Dust Dynamics Around Small Asteroids

William Yu* and Joseph Wang†
*University of Southern California, Los Angeles, California, 90089, USA*
Daoru Han‡
*Worcester Polytechnic Institute, Worcester, Massachusetts, 01609, USA*

**Dynamics of dust transport around an airless body has been a focused area of research in recent years, however, various challenging aspects still remain to be addressed. This paper presents an investigation of charged dust transport and distribution around small asteroids utilizing a full particle Particle-in-Cell (PIC) model to simulate plasma flow around an asteroid and calculate surface charging self-consistently from charge deposition on asteroid. Material properties of asteroid are also explicitly included in the simulation. PIC simulation results are fed into a 3D dust dynamics model to simulate charged dust levitation, transport and distribution. In addition to electrostatic and gravitational forces, the dynamics of dust surface impacts and asteroid body rotation are also included in the model. We discuss the effects on dust levitation and transport by comparing dust grain charge-mass ratio, local electrostatic field and dust grain size. We present simulation results of dust distribution around small spherical asteroids. The study highlights the sensitivity to electrostatic field and grain characteristics while following the general trend that gravity dominates in the far field, where as local electric field prevails at low altitude.**

## Nomenclature

| | |
|---|---|
| $\boldsymbol{g_a}$ | Gravity of asteroid, m/s$^2$ |
| $\mathbf{\Phi}$ | Electric potential, V |
| $\mathbf{B}$ | Magnetic Field, T |
| $\mathbf{E}$ | Electric Field, V/m |
| $\mathbf{F_{SRP}}$ | Solar radiation pressure, Pa |
| $\mathbf{v}$ | Particle velocity, m/s |
| $\mathbf{x_d}$ | Position vector of dust grain from asteroid center, m |
| $\mathbf{x}$ | Particle position, m |
| $\mu$ | Standard gravitational parameter, m$^3$/s$^2$ |
| $\rho$ | Space charge density, m$^{-3}$ |
| $\varepsilon$ | Relative dielectric permittivity |
| $G$ | Universal gravitational constant |
| $m_d$ | Mass of dust grain, kg |
| $q$ | Particle charge, C |
| $Q_d$ | Charge of dust grain, C |
| $r_d$ | Radius of dust grain, m |
| $U_m$ | Gravitational potential, J/kg |

*Research Assistant, Department of Astronautical Engineering, University of Southern California, Los Angeles, California, USA.
†Associate Professor, Department of Astronautical Engineering, University of Southern California, Los Angeles, California, USA.
‡Assistant Research Professor, Mechanical Engineering Department, Worcester Polytechnic Institute, Worcester, Massachusetts, USA.

# I. Introduction

Interactions between plasma and charged dust grains are ubiquitous throughout the solar system, interplanetary medium, and interstellar medium. More specifically, a dusty plasma environment, consists of a quasi-neutral gas of ions and electrons with an additional charged micron-sized particulates, is relevant to explorations on lunar and asteroidal surfaces. In the absence of a global magnetic field and an atmosphere, airless bodies are directly exposed to solar wind plasma and solar irradiation bombardment onto dielectric surfaces. While the source and collisional history of asteroid regolith may be quite different from the process on the lunar surface, the presence of fine particles is evident and a tenuous dust cloud is predicted to envelop all asteroids.[1] During the Apollo era, dust on the Moon caused serious problems for exploration activities including vision obscuration, false instrument readings, dust coating and contamination, loss of traction, clogging of mechanisms, abrasion, thermal control problems, seal failures, and inhalation and irritation.[2] Dust mitigation is a priority for future operations on airless extraterrestrial regolith surfaces. Furthermore, relative to the lunar environment, surface electric fields and solar radiation pressure will have a greater influence on dust dynamics due the the weak local gravity of small asteroids. Regolith exposure to ambient plasma and ultraviolet radiation result in electrostatic charging and dust transport.[3]

Previous studies have examined dust levitation on the lunar surface[4–6] and dust transport on asteroids.[7–10] Current transport models for charged dust grains are limited in the following:

- assumes a specific local plasma charging environment,
- limits simulation domain to two-dimensions,
- utilizes point source approximation for gravitational field,
- surface potential are not solved self-consistently from plasma-asteroid interactions,
- assumes isolated dust grain charging (dust-in-plasma).

In order to accurately model the dynamics of charged dust grains globally, it is necessary to incorporate local plasma-surface interactions to determine asteroid surface charging in a 3D simulation domain with a sophisticated gravity field representation. In this paper, we present a numerical investigation to model dust dynamics around small asteroids. It is crucial to realistically characterize the dusty environment such that spacecraft components and science measurements may be designed more effectively. Dust mobilization and distribution in the circumasteroidal zone are sensitive to parameters such as grain charge-mass ratio, $Q_d/m_d$, local electric field, $\mathbf{E}$, and grain radius, $r_d$. Section II discusses the implementation of a 3D IFE-PIC plasma flow simulation code and a 3D dust transport simulation. Section III presents the numerical results and comparison of the simulation parameters.

# II. Numerical Model and Simulation Considerations

## A. 3D IFE-PIC Plasma Simulation Model

The scope of this study considers a spherical asteroid with a dusty layer regolith immersed in a drifting solar wind plasma flow field at 1 AU. Initial surface floating potential are solved self-consistently by implementing a three-dimensional immersed finite element (IFE), fully kinetic particle-in-cell (PIC) plasma code recently developed by Han et al.[11,12] Plasma field and surface interactions are driven by current balance from solar wind electrons, solar wind ions and photoelectrons induced by ultraviolet radiation. This model treats asteroid surface as an "interface" between 2 mediums with the capability to handle complex geometric topography for charge deposition. Under average solar wind conditions at 1AU, ambient plasma are considered collisionless and unmagnetized, equation of motion of charged particles are governed by Eq. (1),

$$\mathbf{F} = q(\mathbf{E} + \mathbf{v}\times\mathbf{B}) = m\frac{d\mathbf{v}}{dt} = m\frac{d^2\mathbf{x}}{dt^2} \tag{1}$$

where $\mathbf{F}$ is force, $q$ is the electric charge of the particle, $\mathbf{v}$ and $\mathbf{x}$ are the particle velocity and position vector. Electric field $\mathbf{E}$ and potential field $\mathbf{\Phi}$ are solved self-consistently by poisson's equation,

$$\nabla\cdot(\varepsilon\mathbf{E}) = -\nabla\cdot\varepsilon\nabla\mathbf{\Phi} = \rho \tag{2}$$

where $\varepsilon$ is the asteroid relative dielectric permittivity and $\rho$ is the space charge density. Background magnetic field $\mathbf{B}$ is neglected and the regolith relative permittivity is assumed to be 4, compatible with with carbonaceous chondrites.[13–15] Further details of the simulation parameters can be referenced from the recent work of Han et al. and Yu et al.[16,17]

### B. 3D Gravity Field Model

When a dust grain is sufficiently far away from the asteroid, it is appropriate to implement a zeroth-order model for the gravity field. Existing dust transport models assume a spherical, homogenous body by applying a point source approximation:

$$\boldsymbol{g_a}(\mathbf{r}) = -\frac{\mu}{r^3}\mathbf{r}, \tag{3}$$

where $\mathbf{r}$ is the distance from dust to asteroid center of mass. However, near the asteroid, the effects from an irregular shape and non-homogenous internal density on gravitational force cannot be ignored. Developing an accurate gravity field model of asteroids is a challenging astrodynamics task. Conventional approaches to gravity-modeling include spherical and ellipsoidal harmonic expansion series yield very good approximation, provided the field of interest is outside of the minimum circumscribing (Brillouin) sphere of the body. Unfortunately, due to the variability of internal density and irregularities of small asteroid bodies ($\leq 1$ km), classical harmonic expansion model have limited application with errors demonstrated exceeding 100%.[18,19] Methodology developed by Park et al., a finite-element (FE) mass concentration (MASCON) model of the asteroid gives validity of the local gravity within the Brillouin sphere and near surface, along with the capability to establish a non-uniform interior mass distribution.[20] The FE MASCON model utilizes discrete spherical mass elements represented as point sources. The relative positions between elements are fixed and rotate in circular motion about a common axis with constant angular velocity. Finite-element positions are denoted as $\boldsymbol{\rho_i}$, mass elements are denoted as $m_i$, for $i = 1, 2, 3, ..., N$ where $N$ is the total number of elements, and the external gravitational acceleration is given by

$$\nabla U_m = \frac{\partial U}{\partial \mathbf{r}} = -\sum_{i=1}^{N} \frac{Gm_i}{||\mathbf{r} - \boldsymbol{\rho_i}||^3}(\mathbf{r} - \boldsymbol{\rho_i}) \tag{4}$$

The 1 km sized spherical asteroid is modeled by 5975 uniform elements in a hexagonal close packing scheme for a packing density of $\sim 74\%$. This implies an asteroid with uniform microporosity of $\sim 26\%$ and a bulk density of 2.22 g/cm$^3$. A reasonably accurate can be achieved with a modest computational demand, within 1% error for far field and within 10% error near the surface.[21]

### C. 3D Dust Transport Model

For collisionless, unmagnetized drifting plasma, the equation of motion that governs dust levitation and transport is given by

$$m_d \frac{d\mathbf{v_d}}{dt} = Q_d(t)[\mathbf{E}(\mathbf{x_d}) + \mathbf{v_d} \times \mathbf{B}(\mathbf{x_d})] + m_d \cdot \boldsymbol{g_a}(\mathbf{x_d}) + \mathbf{F_{SRP}}(\mathbf{x_d}) \tag{5}$$

where $m_d$, $\mathbf{x_d}$, $\mathbf{v_d}$, and $Q_d(t)$ is the dust grain mass, position vector, velocity vector, and charge, respectively. The steady-state plasma field parameters, $\mathbf{E}(\mathbf{x_d})$ and $\mathbf{\Phi}(\mathbf{x_d})$, are determined by the IFE-PIC plasma simulation, dust charge state, $Q_d(t)$, is constrained by laboratory measurements,[22] and the gravitational field, $\boldsymbol{g_a}(\mathbf{x_d})$, is calculated by the FE MASCON model. Lastly, solar radiation pressure is expressed as Eq. (6)

$$\mathbf{F_{SRP}}(\mathbf{x_d}) = \beta \frac{\mu_s}{a^2}\hat{\boldsymbol{\imath}} \tag{6}$$

$$\beta = \frac{3L_s}{16\pi\mu_s}\frac{\mathrm{Q_{pr}}}{\rho_d r_d} = 5.77\mathrm{x}10^{-5}\frac{\mathrm{Q_{pr}}}{\rho_d r_d} \tag{7}$$

where the dimensionless quantity $\beta$ is a function of solar luminosity $L_s$ at solar distance $a$. Dust properties are defined as grain density $\rho_d$, grain radius $r_d$, and radiation pressure optical coefficient $\mathrm{Q_{pr}}$. Typically, $\mathrm{Q_{pr}} = 1$, assuming complete radiation absorption.[23,24] A summary of the baseline simulation parameters are shown in Table 1. Charged dust simulation particles were uniformly sampled from the spherical surface with zero initial velocity at every time step. It is important to note here that charging measurements were observed

on a "dusty surface layer", rather than a "dust-in-plasma." The distinction must be made as particles on a dusty surface are packed closely to neighboring grains, resulting in a collective plasma sheath, leading to a drastically different current collection onto the grain. In contrast, "dust-in-plasma" is characterized by long inter-grain separation such that each individual grain have its own sheath.

Table 1: Asteroid and grain characteristic parameters

| | | | |
|---|---|---|---|
| **Asteroid geometry** | | spherical, 1 km | |
| **Solar distance** | | 1 A.U. (NEA) | |
| **bulk density** | 1.8 g/cm$^3$ | **grain density** | 3.0 g/cm$^3$ |
| **coeff. of restit.** | 0.8 | **grain size** | 20 $\mu$m |
| **rot. period** | 7.6 hrs | **dielec. const.** | 4.0 |

## III. Results and Discussion

The baseline density contours at steady-state from 3D IFE-PIC plasma simulation for solar wind electrons, solar wind ions, and photoelectrons, are shown in figures 1(a)-1(c), respectively. Results of the plasma potential flow field in figure 1(d) are compatible with plasma expansion theory and lunar observations, where the dayside charges positively due to the prevalence of photoelectrons, while the nightside charging is dominated by energetic electrons.[25–28] The transition between positive and negative potential is evident in figure 2 electrostatic vector field and contour. In the next section, comparisons between dust distribution will illustrate the influence of three parameters that affect mobilization of the regolith.

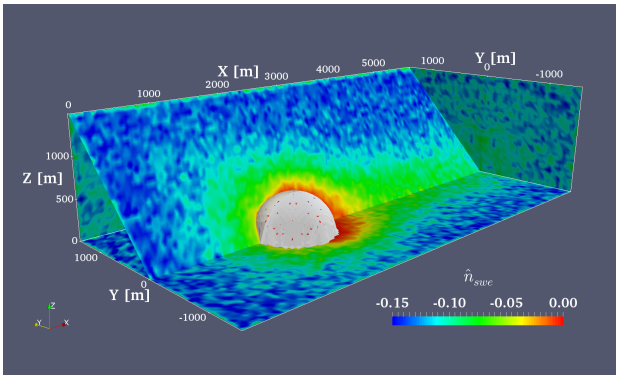


(a) Average solar wind electrons

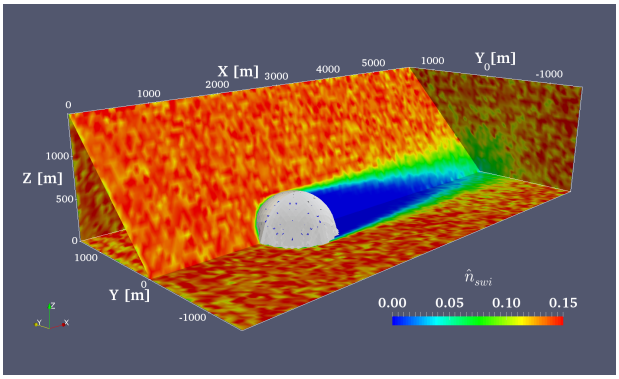


(b) Average solar wind ions

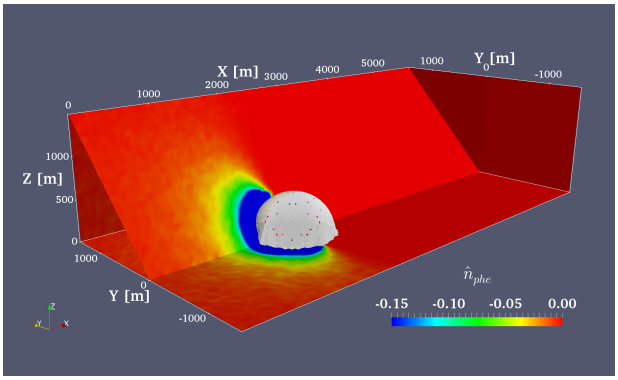


(c) Illuminated photoelectron

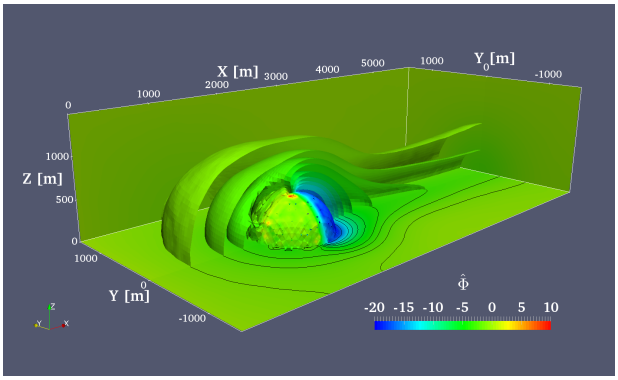


(d) Potential field contour

Figure 1: Density contours of average solar wind plasma, uv-induced photoelectron, and plasma potential field

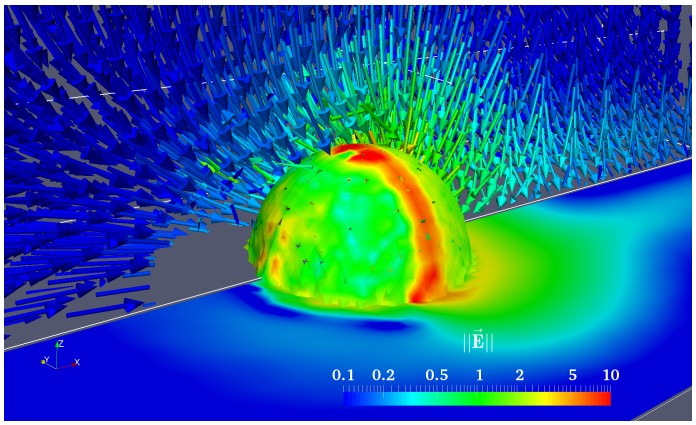


Figure 2: Electrostatic vector field around asteroid

### A. Charge-mass Ratio Comparison

The first parameter under consideration is the initial charge-mass ratio of a levitated grain. First, the baseline case $\|Q/m\| \leq 5\times10^{-5}$ C/kg was calculated from laboratory measurements, while in the second case, the charge-mass ratio is artificially doubled to $\|Q/m\| \leq 1\times10^{-4}$ C/kg. By inspection of Eq. (5), doubling $\|Q/m\|$ effectively doubles the Lorentz force acting on the charged dust. In both cases as shown in figure 3, dust grains near the surface migrate towards the dayside. With a lower charge-mass ratio, more grains appear to be reaching higher altitudes, with greater proportions drifting towards the dayside. An increase in charge-mass also yields greater symmetry in the distribution. Figure 4 is a time-averaged distribution profile as a function of altitude. There are two distinct distribution trends, at low and at high altitudes. Near the surface, dust grains follow an exponential distribution, expressed in Eq.(8), which is analogous to observed atmospheric scaling in neutral gases. As altitudes increases, exponential scaling breaks down, giving rise to a power law distribution given in Eq. (9), converging towards a power of $a$ = -2, or an inverse square relations, as expected for a gravity dominated region. It is interesting to note that an increase charge-mass ratio further perturbs the transition in the density profile from low to high altitude.

$$n(z) = n_0 \exp(-z/z_0) \tag{8}$$

$$n(z) = c_0 z^a \tag{9}$$

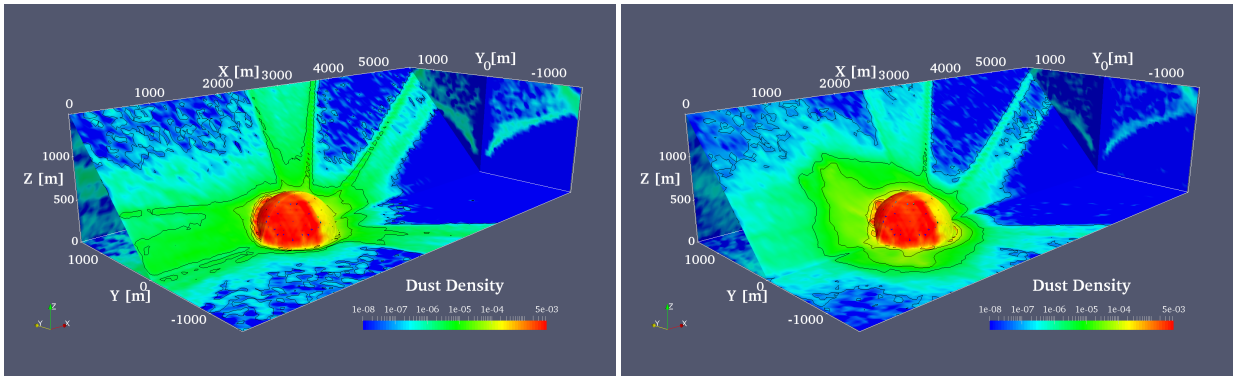


(a) $\|Q/m\| \leq 5\times10^{-5}$ C/kg

(b) $\|Q/m\| \leq 1\times10^{-4}$ C/kg

Figure 3: Dust distribution comparison between 2 charge-mass ratio

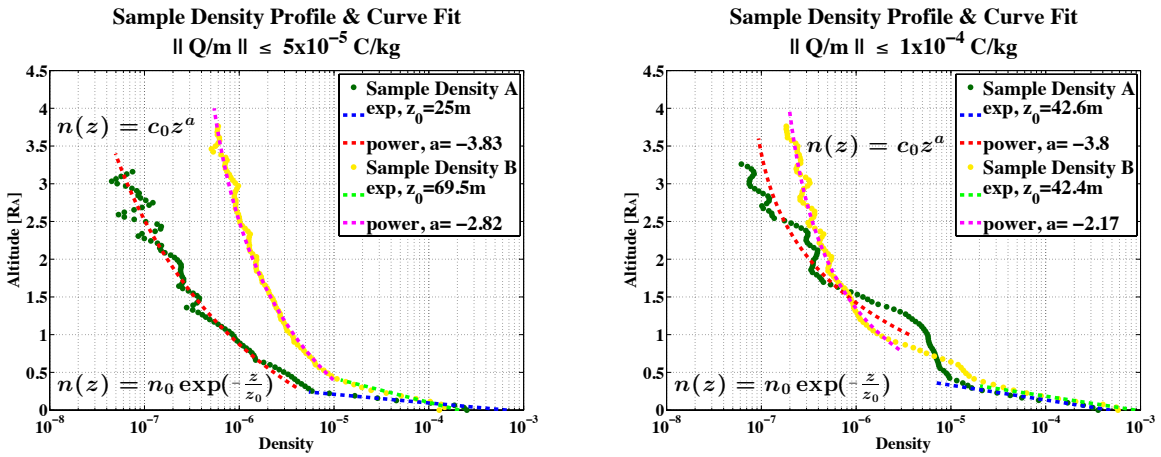


(a) $\|Q/m\| \leq 5\times10^{-5}$ C/kg (b) $\|Q/m\| \leq 1\times10^{-4}$ C/kg

Figure 4: Dust profile vs. altitude between 2 charge-mass ratio

## B. Influence of Photoelectrons

In the absence of direct uv radiation on the dielectric surface, photoelectrons will not be generated, reducing the number of electrons on the dayside. By eliminating the photoelectron species, the electric field is effectively attenuated near the surface, particularly on the side facing the Sun. As a result, figure 5 illustrates that fewer dust grains drift towards the Sun facing hemisphere and the spatial distribution is more spherically symmetric at greater altitude. Dust profile without photoelectrons have a smoother transition between low and high altitude, in addition, distribution converges more closely to the inverse square law (fig. 6). This suggests that as the electric field is weakened, gravity further dominates the transport of charged dust grains.

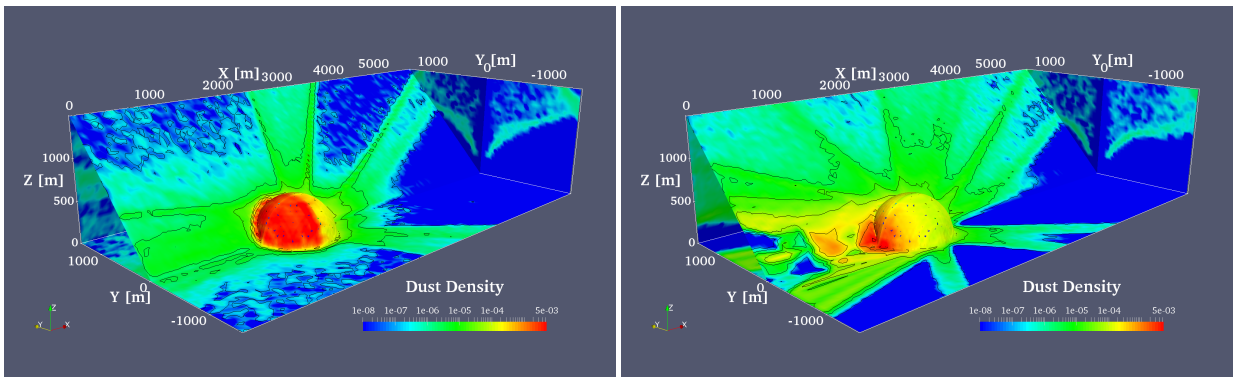


(a) With photoelectrons (b) No photoelectrons

Figure 5: Dust distribution comparison between the presence and absence of photoelectrons

## C. Dust Grain Size

While maintaining spherical dust grains, modifications on grain diameter can severely influence the dynamics of dust transport. A decrease in grain size reduces the surface area for current collection in addition to reducing the particle mass. For the purposes of this comparison, the charge state of the grain is kept constant and only mass will be the affected parameter. A reduction in grain size by 1000 effectively increases the charge-mass ratio by 3 orders of magnitude. In a comparison between the two dust grain sizes (figure 7), it is apparent that the smaller grains are more readily ejected from the surface. Furthermore, the ejection of dust from the asteroid body migrate downstream with flow of plasma rather than upstream as with the

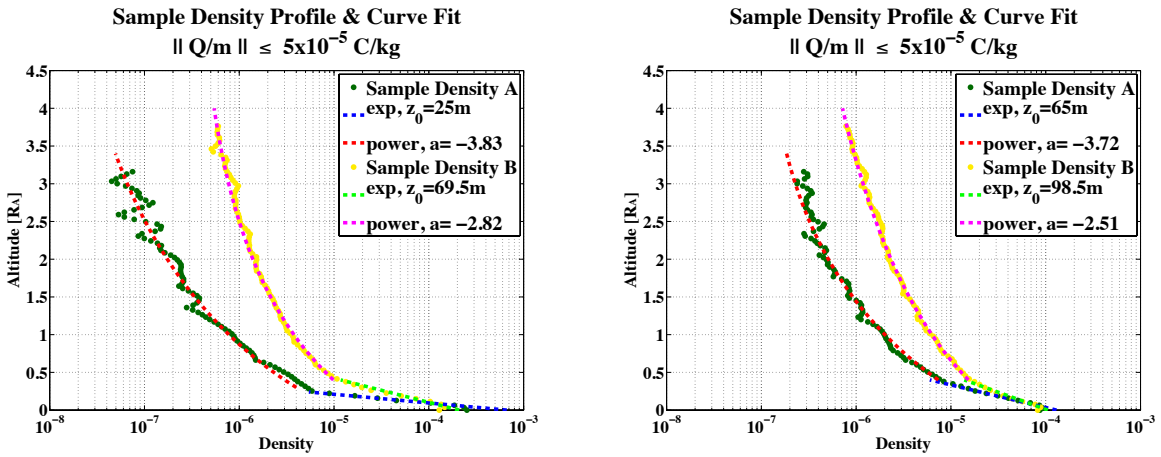


(a) With photoelectrons (b) No photoelectrons

Figure 6: Dust profile vs. altitude between the presence and absence of photoelectrons

baseline case. It may be possible that solar radiation pressure are much more efficient at sweeping away fine grains where as electrostatic forces are more effective on larger particles. This is in agreement with previous speculations on the role of solar radiation pressure relative to interplanetary grains.[7,23]

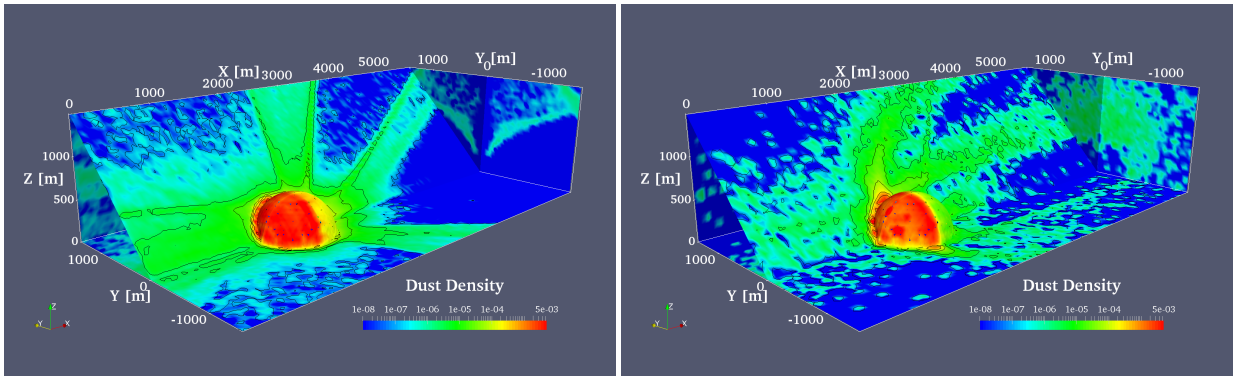


(a) Grain size: 20 $\mu$m (b) Grain size: 20 nm

Figure 7: Dust distribution comparison between 2 grain sizes

## IV. Conclusion

We have presented a numerical investigation on dust distribution around small spherical asteroids with the implementation of a 3D IFE-PIC plasma-asteroid interaction model and a 3D dust transport model. In all simulation cases, charged dust tend to migrate toward the dayside at high altitudes, with the exception of the ultra fine grain case. Near the surface, there is a preference to gravitate towards the dayside. At large altitudes, gravity appears to be the dominant player in dust transport, while the electric field has a strong influence on dust dynamics at low altitudes. An increase in the electrostatic force is more efficient at perturbing the density profile between the low and high altitude. For smaller grains, solar radiation pressure may have a greater role on dynamics around an asteroid. This work successfully implemented an FE MASCON gravitational model. Future work will investigate further into the role of the asteroid shape and internal structure of the airless body.

# References


[1]Horányi, M., Szalay, J., Kempf, S., Schmidt, J., Grün, E., Srama, R., and Sternovsky, Z., "A permanent, asymmetric dust cloud around the Moon," *Nature*, Vol. 522, No. 7556, 2015, pp. 324–326.

[2]Stubbs, T., Vondrak, R., and Farrell, W., "Impact of Dust on Lunar Exploration," *Dust in Planetary Systems*, Vol. 643, 2007, pp. 239–243.

[3]Rennilson, J. and Criswell, D., "Surveyor observations of lunar horizon-glow," *The Moon*, Vol. 10, No. 2, 1974, pp. 121–142.

[4]Colwell, J., Robertson, S., Horányi, M., Wang, X., Poppe, A., and Wheeler, P., "Lunar Dust Levitation," *Journal of Aerospace Engineering*, Vol. 22, No. 1, 2009, pp. 2–9.

[5]Poppe, A. and Horányi, M., "Simulations of the photoelectron sheath and dust levitation on the lunar surface," *Journal of Geophysical Research, Space Physics*, Vol. 115, No. A8, 2010, A08106.

[6]Collier, M., Farrell, W., and Stubbs, T., "The lunar dust pendulum," *Advances in Space Research*, Vol. 52, No. 2, 2013, pp. 251–261, Lunar Exploration - II.

[7]Lee, P., "Dust Levitation on Asteroids," *Icarus*, Vol. 124, No. 1, 1996, pp. 181–194.

[8]Colwell, J., Gulbis, A., Horányi, M., and Robertson, S., "Dust transport in photoelectron layers and the formation of dust ponds on Eros," *Icarus*, Vol. 175, No. 1, 2005, pp. 159 – 169.

[9]Hughes, A., Colwell, J., and DeWolfe, A., "Electrostatic dust transport on Eros: 3-D simulations of pond formation," *Icarus*, Vol. 195, No. 2, 2008, pp. 630–648.

[10]Hartzell, C. and Scheeres, D., "Dynamics of levitating dust particles near asteroids and the moon," *Journal of Geophysical Research: Planets*, Vol. 118, No. 1, 2013, pp. 116–125.

[11]Han, D., *Particle-in-Cell Simulations of Plasma Interactions with Asteroidal and Lunar Surfaces*, Ph.D. thesis, University of Southern California, Los Angeles, California, 2015.

[12]Han, D., Wang, P., He, X., Lin, T., and Wang, J., "A 3D immersed finite element method with non-homogeneous interface flux jump for applications in particle-in-cell simulations of plasmalunar surface interactions," *Journal of Computational Physics*, Vol. 321, 2016, pp. 965–980.

[13]Sarma, S., Subba Rao, T., and Mautner, M., "Electrical properties of Murchison carbonaceous chondrite meteorite," *Balkan Physics Letters*, Vol. 12, No. 1, 2004, pp. 31–37.

[14]Vilas, F., "Spectral Characteristics of Hayabusa 2 Near-Earth Asteroid Targets 162173 1999 JU3 and 2001 QC34," *The Astronomical Journal*, Vol. 135, No. 4, 2008, pp. 1101–1105.

[15]Calla, O. and Rathore, I., "Study of complex dielectric properties of lunar simulants and comparison with Apollo samples at microwave frequencies," *Advances in Space Research*, Vol. 50, No. 12, 2012, pp. 1607 – 1614.

[16]Han, D., Wang, J., and He, X., "A Nonhomogeneous Immersed-Finite-Element Particle-in-Cell Method for Modeling Dielectric Surface Charging in Plasmas," *IEEE Transactions on Plasma Science*, Vol. 44, No. 8, 2016, pp. 1326–1332.

[17]Yu, W., Han, D., and Wang, J., "Numerical Dust Distribution around Small Asteroids," Manuscript submitted for publication.

[18]Werner, R. and Scheeres, D., "Exterior gravitation of a polyhedron derived and compared with harmonic and mascon gravitation representations of asteroid 4769 castalia," *Celestial Mechanics and Dynamical Astronomy*, Vol. 65, No. 3, 1997, pp. 313–344.

[19]Casotto, S. and Musotto, S., "Methods for computing the potential of an irregular, homogeneous, solid body and its gradient," *Astrodynamics Specialist Conference, Guidance, Navigation, and Control and Co-located Conferences*, American Institute of Aeronautics and Astronautics, Aug. 2000.

[20]Park, R., Werner, R., and Bhaskaran, S., "Estimating Small-Body Gravity Field from Shape Model and Navigation Data," *Journal of Guidance, Control, and Dynamics*, Vol. 33, No. 1, 2010, pp. 212–221.

[21]Ren, Y. and Shan, J., "On tethered sample and mooring systems near irregular asteroids," *Advances in Space Research*, Vol. 54, No. 8, 2014, pp. 1608–1618.

[22]Yu, W., Wang, J., and Chou, K., "Laboratory Measurement of Lunar Regolith Simulant Surface Charging in a Localized Plasma Wake," *Plasma Science, IEEE Transactions on*, Vol. 43, No. 12, Dec 2015, pp. 4175–4181.

[23]Burns, J., Lamy, P., and Soter, S., "Radiation forces on small particles in the solar system," *Icarus*, Vol. 40, No. 1, 1979, pp. 1 – 48.

[24]Hamilton, D. and Burns, J., "Orbital stability zones about asteroids: II. The destabilizing effects of eccentric orbits and of solar radiation," *Icarus*, Vol. 96, No. 1, 1992, pp. 43–64.

[25]Halekas, J., Lin, R., and Mitchell, D., "Large negative lunar surface potentials in sunlight and shadow," *Geophysical Research Letters*, Vol. 32, No. L09102, 2005.

[26]Farrell, W., Stubbs, T., Vondrak, R., Delory, G., and Halekas, J., "Complex electric fields near the lunar terminator: The near-surface wake and accelerated dust," *Geophysical Research Letters*, Vol. 34, No. L14201, 2007.

[27]Halekas, J., Delory, G., Lin, R., Stubbs, T., and Farrell, W., "Lunar Prospector observations of the electrostatic potential of the lunar surface and its response to incident currents," *Journal of Geophysical Research*, Vol. 113, No. A09102, 2008.

[28]Halekas, J., Saito, Y., Delory, G., and Farrell, W., "New views of the lunar plasma environment," *Planetary and Space Science*, Vol. 59, No. 14, 2011, pp. 1681 – 1694.